APL MATERIALS **3**, 062511 (2015)

Comparison of topotactic fluorination methods for complex oxide films

E. J. Moon,[1,a] A. K. Choquette,[1] A. Huon,[1] S. Z. Kulesa,[1] D. Barbash,[2] and S. J. May[1,b]
[1]*Department of Materials Science and Engineering, Drexel University, Philadelphia, Pennsylvania 19104, USA*
[2]*Centralized Research Facilities, Drexel University, Philadelphia, Pennsylvania 19104, USA*

(Received 27 February 2015; accepted 10 May 2015; published online 26 May 2015)

We have investigated the synthesis of $SrFeO_{3-\alpha}F_{\gamma}$ (α and $\gamma \leq 1$) perovskite films using topotactic fluorination reactions utilizing poly(vinylidene fluoride) as a fluorine source. Two different fluorination methods, a spin-coating and a vapor transport approach, were performed on as-grown $SrFeO_{2.5}$ films. We highlight differences in the structural, compositional, and optical properties of the oxyfluoride films obtained via the two methods, providing insight into how fluorination reactions can be used to modify electronic and optical behavior in complex oxide heterostructures. [http://dx.doi.org/10.1063/1.4921579]

Topotactic reactions, in which a chemical transformation occurs while maintaining the crystalline framework of a material,[1] have garnered increasing interest within the oxide heterostructure community as a means to expand the compositional range accessible for epitaxial films. These reactions, performed on films post-deposition, have proven valuable in altering the anion occupation or composition of oxide heterostructures. One example is reversible oxidation and reduction, which can be carried out at lower temperatures and on shorter time scales than in bulk materials due to the reduced volume of thin films. For example, post-growth anneals in oxygen, dilute O_3/O_2 mixtures, vacuum, or forming gas mixtures have been used to oxidize or reduce, depending on the annealing environment, many $ABO_{3-\delta}$ perovskites to achieve a targeted anion stoichiometry, typically $\delta = 0$ or 0.5.[2–11] The use of aggressive reducing agents, such as Ca_2H,[12] has enabled the realization of ABO_2 compounds such as $SrFeO_2$ and $LaNiO_2$ via topotactic transformations from as-grown ABO_3 and $ABO_{2.5}$ films.[13,14] Given the sensitive coupling between δ and physical properties,[15–17] topotactic oxidation and reduction reactions have been used to induce large changes to the electronic, optical, and magnetic properties of epitaxial films[18–20] and may prove applicable in ionically controlled solid state devices.[21–24]

A second class of topotactic reaction involves the insertion or substitution of a different anion on the oxygen site to stabilize mixed-anion perovskites such as oxyfluorides.[25] Our motivation for synthesizing oxyfluorides is twofold. First, the substitution of F^- for O^{2-} will electron dope the material, thus enabling a route to reduce the *B*-site valence state without resorting to the introduction of oxygen vacancies. Second, the resultant *B*–F bonds will be more ionic than the *B*–O bonds. These changes to the *B*-site electron count and the *B*-anion bond covalency are dual mechanisms by which the functional properties of perovskite films can be engineered.

Previous work on bulk $SrFeO_2F$ and $SrFeO_3$ illustrates some of the physical differences between oxyfluorides and oxides with the same cation composition. $SrFeO_3$ exhibits metallic conductivity with a nominal Fe^{4+} valence.[17] The substitution of F^- for O^{2-} in $SrFeO_2F$ adds an electron to the system, reducing the Fe oxidation state to 3+.[26–28] Consistent with reduction of the

[a]em582@drexel.edu
[b]smay@coe.drexel.edu

Fe cation, a lattice expansion is observed upon fluorinating $SrFeO_3$ (a = 3.851 Å)[29] to $SrFeO_2F$ (a = 3.955 Å),[26–28] both of which are cubic. Unlike $SrFeO_3$, in which helical magnetic ordering is observed below 130 K,[30] $SrFeO_2F$ is a robust G-type antiferromagnet with a Neel temperature of 685-710 K.[31–33] The spin structure and high ordering temperature are consistent with $LaFeO_3$ and the brownmillerite $SrFeO_{2.5}$, which also exhibit Fe in high spin d^5 configurations strongly favoring antiferromagnetic superexchange interactions.[34,35]

Recent work has demonstrated fluorination of epitaxial perovskites via the thermal decomposition of fluorine-containing polymers in close proximity to a $ABO_{3-\delta}$ film,[36,37] a technique adapted from fluorination processes carried out on bulk oxides.[26,38,39] In one approach, a poly(vinylidene fluoride) (PVDF) solution is spin-coated onto an as-grown, oxygen deficient film.[36] The oxide/polymer bilayer is then annealed in flowing O_2 to decompose the polymer, enabling F ions to diffuse into the film. In a second approach, PVDF is placed in a heated tube furnace upstream from the perovskite film.[37] A carrier gas is used to transport vapor from the PVDF to the film, resulting in F incorporation. Both approaches have been used to stabilize $SrFeO_{3-\delta}F_\gamma$ (SFO-F)films. While the methods are similar in nature, differences in process temperature, carrier gas, and time result in key distinction between the films obtained from the two approaches. The aim of this work is to compare $SrFeO_{3-\delta}F_\gamma$ films obtained via these two approaches, highlighting the relative advantages of each reaction method, and to discuss ongoing challenges and opportunities in topotactic fluorination of epitaxial perovskite films.

Oxygen deficient ferrite films, $SrFeO_{3-\delta}$ (SFO), were grown with oxide molecule beam epitaxy (MBE) using an interrupted growth mode on $SrTiO_3$ (STO) substrates. During deposition, the substrate temperature was held at 600 °C, and O_2 was sourced to the substrate at a rate that yielded a chamber pressure of $\sim 1.1 \times 10^{-5}$ mbar. The thickness of the films was approximately 23 nm (~60 unit cells; uc). The spin-coating (SC) and vapor transport (VT) fluorination processes, which are described below, were carried out using PVDF (Sigma-Aldrich, CH_2CF_2, 1.78 g/ml at 25 °C). Following the fluorination, x-ray diffraction (XRD) measurements were taken around the (0 0 2) truncation rod of the film using a Rigaku SmartLab diffractometer, equipped with parabolic mirror and two bounce monochromators on the incident and diffracted beams. X-ray photoelectron spectroscopy (XPS) depth profiling was performed with a ThermoFisher K-Alpha spectrometer using a monochromated Al Kα source with a pass energy of 20 eV at Rutgers University and with a PHI spectrometer with a pass energy of 23 eV at Drexel University. For sputter depth profiling, Ar+ ions of 2 keV energy at a sputtering spot size of 2×2 mm^2 and a 60 s sputter interval were used. Optical absorption spectra were measured using variable angle spectroscopic ellipsometer (J.A. Woollam M-2000U). Data were collected at 5 incident angles (65°, 67.5°, 70°, 72.5°, and 75°) in order to improve the data fitting using a Levenberg-Marquardt algorithm of Lorentz oscillators in WVASE software. All ellipsometry measurements were taken at room temperature.

The SC fluorination process [Fig. 1(a)] has been previously reported in Ref. 36. The film is spin-coated with a solution of PVDF (10 wt. % in dimethylformamide (DMF)), which is followed by a heat treatment in a quartz tube under a slow O_2 flow at 600 °C for 2 h. The presence of O_2 during the annealing step of the SC process facilitates the removal of the by-products produced during thermal decomposition of the PVDF. In contrast, when the SC process was performed under a N_2 gas flow, a black residue remained on the film following the anneal and no film peaks were present in x-ray diffraction. Figure 1(b) illustrates the VT fluorination process, which we adapted from Katayama *et al.*[37] In this approach, fluorination is carried out by heating a perovskite film and PVDF pellets in a quartz tube for 24 h under a flowing carrier gas; here, we use N_2 and Ar. The film is placed in the quartz tube downstream from the PVDF pellets.

Figure 2 shows XRD measurements taken around the pseudocubic (0 0 2) truncation rod of strontium ferrite films before and after the two different fluorination processes. The c-axis parameter of the as-grown oxygen deficient SFO thin film is found to be ~3.979 Å, as shown in Fig. 2(a), which is comparable to previous reports of brownmillerite $SrFeO_{2.5}$ films on STO.[4,40] The XRD data of the film fluorinated with the VT method at 275 °C in N_2 (hereafter, VT-N_2-275) show a Bragg peak corresponding to a c-axis parameter of ~4.004 Å [Fig. 2(b)]. The fluorinated film by VT in Ar gas at 240 °C (VT-Ar-240) exhibits a diffraction peak of a c-axis parameter ~4.044 Å [Fig. 2(c)]. In the film fluorinated at the lower temperature of 210 °C in Ar gas

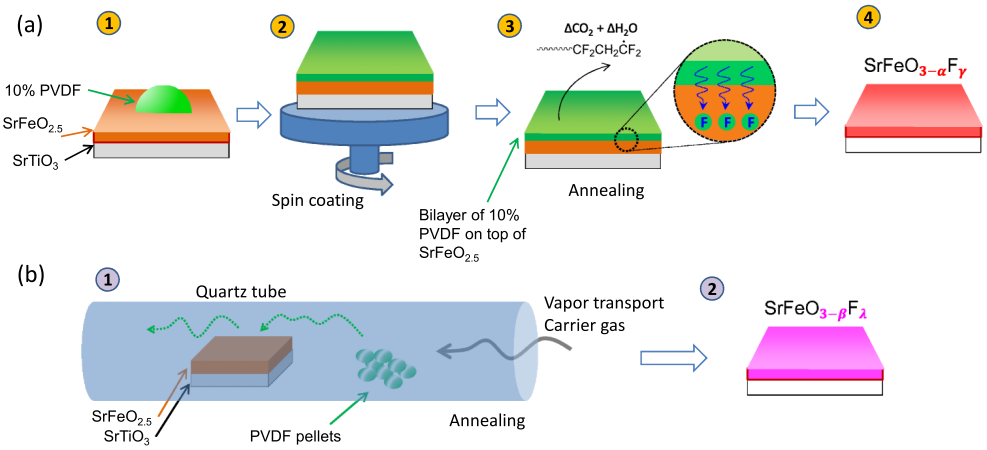

FIG. 1. Schematics of the fluorination processes. (a) Spin-coating process carried out on a bilayer consisting of PVDF and an oxygen-deficient SFO film. A 10% solution of PVDF is first spin-coated onto an oxygen-deficient $SrFeO_{3-\delta}$ film grown on STO (1,2). After the heat treatment of fluorination process (3), $SrFeO_{3-\alpha}F_{\gamma}$ (red) is obtained (4). Green spheres in the inset of (3) represent fluorine atoms diffusing through the polymer film during heat treatment. (b) Vapor transport process carried out on an as-grown oxygen deficient $SrFeO_{3-\delta}$ placed downstream from PVDF pellets in a heated quartz tube in the presence of a flowing carrier gas, resulting in $SrFeO_{3-\beta}F_{\lambda}$ (magenta).

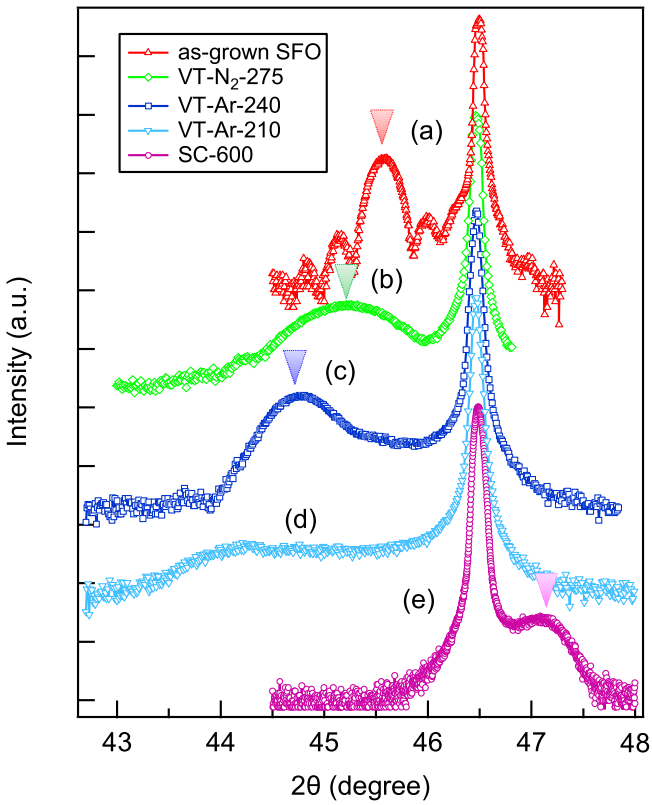

FIG. 2. XRD data of SFO before and after fluorination processes. (a) Oxygen-deficient as-grown SFO, (b) fluorinated SFO-F film obtained from the vapor transport process in N_2 (VT-N_2-275), ((c) and (d)) fluorinated SFO-F film obtained from the vapor transport process in Ar (VT-Ar-210 and VT-Ar-240), and (e) fluorinated SFO-F film obtained from the spin-coating process (SC-600). The (0 0 2) peak is shifted upon fluorinating the as-grown film, resulting in a difference of the c-axis lattice parameters in SFO-F films synthesized via the different processes.

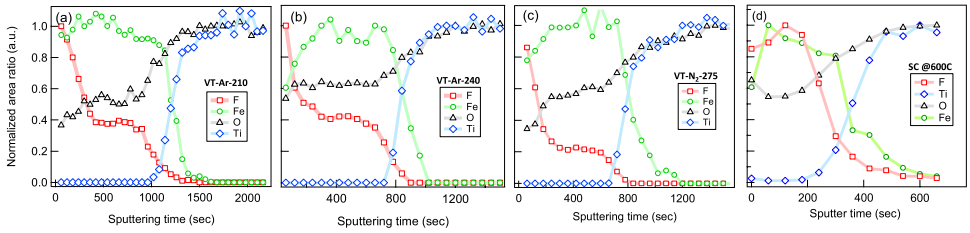

FIG. 3. Normalized concentration depth profiles obtained from XPS for four different SFO-F /STO films. (a) VT-Ar-210 for 24 h, (b) VT-Ar-240 for 24 h, (c) VT-N_2-275 for 24 h, and (d) SC-600 for 2 h. The data in panel (d) are adapted with permission from Moon *et al.*, J. Am. Chem. Soc. **136**, 2224 (2014). Copyright 2014 American Chemical Society.

(VT-Ar-210), the Bragg peak is shifted further to a lower angle than the VT-Ar-240 film, but with much weaker intensity and significant peak broadening [Fig. 2(d)]. We note that the VT process is very sensitive to the processing temperature. Films fluorinated in flowing N_2 did not exhibit a Bragg peak when the process was carried out below 240 °C or above 300 °C. Similarly, Bragg peaks were not observed for VT-processed films in flowing Ar for annealing temperatures above 275 °C. Therefore, we find that the choice of carrier gas alters the optimal temperature range for the VT process. In contrast to the VT fluorination process, the film (0 0 2) peak from SFO-F film synthesized by the SC process (SC-600) appears at a higher angle than that of the STO substrate and its *c*-axis parameter is ~3.855 Å [Fig. 2(d)]. Films processed with the SC method at 400 °C and 800 °C did not exhibit diffraction peaks. The crystalline coherence length (ξ) along the out-of-plane direction for the fluorinated films was obtained from the full-width at half maximum (FWHM) of the (0 0 2) peak using $\xi = 2\pi/\text{FWHM}$, where FWHM is in Å^{-1}. This analysis yields ξ = 12, 18, and 10 nm for the VT-N_2-275, VT-Ar-240, and SC-600 films, respectively, indicating that the crystalline quality of the VT synthesized films is better than that of the SC synthesized films.

The relative fluorine concentration as a function of distance from the surface was measured by XPS depth profile analysis, performed with Ar+ sputtering of the film. Figure 3 shows the depth profiles of the O 1s, F 1s, Fe 2p, and Ti 2p normalized peak intensities. The depth at which the Fe 2p is suppressed and the Ti 2p peak appears indicates the relative location of the film/substrate interface. Figure 3(a) shows the normalized concentration depth profile for the VT-Ar-210 film, revealing a near-surface region with a gradually decreasing F concentration, followed by a region of constant F concentration. Assuming the sputter rate is constant as a function of depth within the film, each of these two regions is ~12 nm. When the VT processing temperature is raised to 240 °C in Ar, the constant F concentration region is increased to ~17 nm, while the near-surface of varying F content becomes less wide (~5 nm), as shown in Fig. 3(b). The depth profile from the VT-N_2-275 sample is shown in Fig. 3(c). This film also exhibits two layers of differing F concentration. The layer with constant F concentration is approximately the same width as that of VT-Ar-240 but with a seemingly lower F concentration. The depth profile of the SC-600 film reveals a more uniform F concentration throughout the film, extending from the surface to a depth of ~15 nm. The carbon 1s peak was also measured after each sputtering cycle to monitor carbon contamination. While the as-fluorinated VT films have a C 1s peak at the surface, the peak is absent after 1 min of sputtering, as shown in supplementary Figure S1(a).[41] The carbon peak was also absent in the SC film after brief sputtering.[36]

We next compare the optical absorption spectra measured from a $SrFeO_3$ film, an as-grown SFO film, and the fluorinated VT-Ar-240 film to elucidate the effect of fluorine doping on optical properties. Figure 4 shows optical absorption spectra as a function of photon energy for these samples at room temperature. The $SrFeO_3$ exhibits strong absorption over the entire measured spectral range. The as-grown oxygen-deficient SFO film shows characteristics of semiconducting behavior, with an absorption edge near 2 eV. Interestingly, the VT-Ar-240 film exhibits a similar optical response to that of the as-grown SFO. The spectra of the VT-N_2-275 sample (not shown) are similar to the VT-AR-240 film. The spectra of as-grown SFO and the VT fluorinated SFO-F films are also qualitatively similar to $LaFeO_3$, in which Fe takes on a 3+ valence state and an absorption edge near 2 eV is observed.[42] With the introduction of Sr to $La_{1-x}Sr_xFeO_3$, which acts to increase the nominal

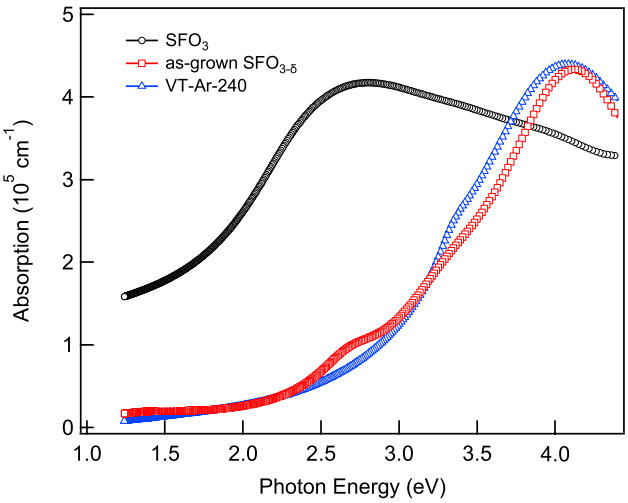

FIG. 4. Optical absorption of $SrFeO_3$ (black), as-grown oxygen deficient SFO (red), and the VT-Ar-240 (blue) films.

Fe valence state above 3+, significant absorption is observed below 2 eV, the magnitude of which increases with increasing Sr content.[42] Therefore, we suggest that the lack of optical absorption below 2 eV in the as-grown SFO and VT processed SFO-F films is indicative of a Fe valence state near 3+. This is consistent with the as-grown SFO having a composition near $SrFeO_{2.5}$. Electrical resistivity measurements were attempted on the as-grown SFO and VT SFO-F films; however, the samples were too resistive to be measured at room temperature. This behavior is again reminiscent of insulating $LaFeO_3$, consistent with a d^5 electronic configuration in the as-grown and VT processed SFO-F films.

Based on the structural, optical, and electrical results, we can clarify the main differences between the VT and SC processes. The large *c*-axis parameter, lack of optical absorption below 2 eV, and highly insulating behavior all suggest a Fe valence of ~3+ in the VT processed SFO films. This would correspond to a nominal composition near $SrFeO_2F$ consistent with the compositional range reported by Katayama *et al.*[37] The properties of the SC processed film, including the reduced *c*-axis parameter and previously reported electrical properties,[36] are consistent with a lower F concentration (a higher Fe valence) than in the VT processed films. The room temperature resistivity of SC-600 films is on the order of 0.1 Ω cm,[36] a value comparable to that measured in a $La_{0.64}Sr_{0.36}FeO_3$ film.[20] This suggests a Fe valence near 3.3-3.4+ in the SC-600 sample. We also note that the lineshape of the Fe 2p XPS peak obtained from the VT and SC films after 1 min of sputtering is also consistent with a lower Fe valence in the VT films compared to the SC film. These XPS data can be found in Fig. S1(b).[41] The higher F concentrations obtained from the VT process may result from the longer duration of fluorine exposure (24 h compared to 2 h). In the SC process, the polymer film is completely burned off by 2 h, thereby setting a limit on the exposure time.

The higher fluorine concentration obtained from VT compared to SC could also result from the ability of PVDF to reduce metal oxides.[39,43] The VT process is carried out in the presence of PVDF in an inert gas, leading to the reduction of the as-grown SFO film. This increases the number of anion vacancies for the F ions to occupy, enabling the formation of $SrFeO_2F$ from a $SrFeO_{2.5}$ film. In contrast, the SC process is performed in flowing O_2, which removes the C and H by-products that would otherwise act to reduce the SFO film. Thus, the SC fluorination process does not appear to significantly increase the number of oxygen vacancies within the as-grown SFO film.

The uniformity of the F concentration within the films is another main difference we observe between the two processes, which we attribute to the difference in anneal temperatures. The higher temperature SC approach yields a more uniform F concentration, while the VT process produces films with greater depth variation of the F content. We note that the ξ values obtained from the VT processed films are in good agreement with the thickness of the region of constant F content. This suggests that the variation in F concentration plays a role in the peak broadening of the VT

processed films. In contrast, ξ is less than the region of uniform F concentration in the SC-600 film, suggesting the reduced crystalline quality is not related to compositional fluctuations.

The use of topotactic reactions holds considerable promise for the realization of mixed-anion perovskite heterostructures, such as the oxyfluorides synthesized in this work. However, numerous challenges and questions remain regarding how to fully harness these fluorination approaches in the service of thin film materials discovery. These include optimizing the processes to increase F uniformity and increase crystalline quality in the fluorinated films, developing conditions to yield tunable F concentrations, and exploring anion ordering in films that exhibit oxygen vacancy ordering prior to fluorination. Additionally, other fluorination methods that have been utilized for bulk materials, such as XeF_2 gas or electrochemical methods,[44,45] remain to be applied to perovskite films and may provide alternative routes to realizing epitaxial perovskite oxyfluorides.

This work was supported by the Army Research Office (No. W911NF-12-1-0132) and the National Science Foundation (No. DMR-1151649). We thank Professor Chris Li for helpful discussions and Professor Caroline Schauer for access to the ellipsometer. Acquisition of the Physical Properties Measurement System was supported by the U. S. Army Research Office under Grant No. W911NF-11-1-0283. The x-ray diffractometer was acquired with funds from NSF MRI Award No. DMR-1040166.

[1] K. G. S. Ranmohotti, E. Josepha, J. Choi, J. Zhang, and J. B. Wiley, Adv. Mater. **23**, 442 (2011).
[2] D. C. Worledge, G. J. Snyder, M. R. Beasley, T. H. Geballe, R. Hiskes, and S. DiCarolis, J. Appl. Phys. **80**, 5158 (1996).
[3] S. Stemmer, A. J. Jacobson, X. Chen, and A. Ignatiev, J. Appl. Phys. **90**, 3319 (2001).
[4] H. Yamada, M. Kawasaki, and Y. Tokura, Appl. Phys. Lett. **80**, 622 (2002).
[5] C. Callender, D. P. Norton, R. Das, A. F. Hebard, and J. D. Budai, Appl. Phys. Lett. **92**, 012514 (2008).
[6] W. S. Choi, Z. Marton, S. Y. Jang, S. J. Moon, B. C. Jeon, J. H. Shin, S. S. A. Seo, T. W. Noh, K. Myung-Whun, H. N. Lee, and Y. S. Lee, J. Phys. D: Appl. Phys. **42**, 165401 (2009).
[7] L. Maritato, A. Galdi, P. Orgiani, J. W. Harter, J. Schubert, K. M. Shen, and D. G. Schlom, J. Appl. Phys. **113**, 053911 (2013).
[8] S. Chakraverty, T. Matsuda, H. Wadati, J. Okamoto, Y. Yamasaki, H. Nakao, Y. Murakami, S. Ishiwata, M. Kawasaki, Y. Taguchi, Y. Tokura, and H. Y. Hwang, Phys. Rev. B **88**, 220405(R) (2013).
[9] H. Jeen, W. S. Choi, J. W. Freeland, H. Ohta, C. U. Jung, and H. N. Lee, Adv. Mater. **25**, 3651 (2013).
[10] Y. J. Xie, M. D. Scafetta, E. J. Moon, A. L. Krick, R. J. Sichel-Tissot, and S. J. May, Appl. Phys. Lett. **105**, 062110 (2014).
[11] K. H. L. Zhang, P. V. Sushko, R. Colby, Y. Du, M. E. Bowden, and S. A. Chambers, Nat. Commun. **5**, 4669 (2014).
[12] Y. Tsujimoto, C. Tassel, N. Hayashi, T. Watanabe, H. Kageyama, K. Yoshimura, M. Takano, M. Ceretti, C. Ritter, and W. Paulus, Nature **450**, 1062 (2007).
[13] S. Inoue, M. Kawai, Y. Shimakawa, M. Mizumaki, N. Kawamura, T. Watanabe, Y. Tsujimoto, H. Kageyama, and K. Yoshimura, Appl. Phys. Lett. **92**, 161911 (2008).
[14] M. Kawai, S. Inoue, M. Mizumaki, N. Kawamura, N. Ichikawa, and Y. Shimakawa, Appl. Phys. Lett. **94**, 082102 (2009).
[15] J. F. Mitchell, D. N. Argyriou, C. D. Potter, D. G. Hinks, J. D. Jorgensen, and S. D. Bader, Phys. Rev. B **54**, 6172 (1996).
[16] R. D. Sanchez, M. T. Causa, A. Caneiro, A. Butera, M. Vallet-Regi, M. J. Sayagues, J. Gonzalez-Calbet, F. Garcia-Sanz, and J. Rivas, Phys. Rev. B **54**, 16574 (1996).
[17] P. Adler, A. Lebon, V. Damljanovic, C. Ulrich, C. Bernhard, A. V. Boris, A. Maljuk, C. T. Lin, and B. Keimer, Phys. Rev. B **73**, 094451 (2006).
[18] F. J. Rueckert, Y. F. Nie, C. Abughayada, S. A. Sabok-Sayr, H. E. Mohottala, J. I. Budnick, W. A. Hines, B. Dabrowski, and B. O. Wells, Appl. Phys. Lett. **102**, 152402 (2013).
[19] W. S. Choi, H. Jeen, J. H. Lee, S. S. A. Seo, V. R. Cooper, K. M. Rabe, and H. N. Lee, Phys. Rev. Lett. **111**, 097401 (2013).
[20] Y. Xie, M. D. Scafetta, R. J. Sichel-Tissot, E. J. Moon, R. C. Devlin, H. Wu, A. L. Krick, and S. J. May, Adv. Mater. **26**, 1434 (2014).
[21] S. V. Kalinin and N. A. Spaldin, Science **341**, 858 (2013).
[22] T. Tsuchiya, K. Terabe, and M. Aono, Appl. Phys. Lett. **103**, 073110 (2013).
[23] J. Shi, Y. Zhou, and S. Ramanathan, Nat. Commun. **5**, 4860 (2014).
[24] M. D. Biegalski, E. Crumlin, A. Belianinov, E. Mutoro, Y. Shao-Horn, and S. V. Kalinin, Appl. Phys. Lett. **104**, 161910 (2014).
[25] C. Greaves and M. Grazia Fracesoni, Curr. Opin. Solid State Mater. Sci. **3**, 132 (1998).
[26] F. J. Berry, X. Ren, R. Heap, P. Slater, and M. F. Thomas, Solid State Commun. **134**, 621 (2005).
[27] O. Clemens, M. Kuhn, and R. Haberkorn, J. Solid State Chem. **184**, 2870 (2011).
[28] C. K. Blakely, J. D. Davis, S. R. Bruno, S. K. Kraemer, M. Zhu, X. Ke, W. Bi, E. E. Alp, and V. V. Poltavets, J. Fluorine Chem. **159**, 8 (2014).
[29] M. Reehuis, C. Ulrich, A. Maljuk, Ch. Niedermayer, B. Ouladdiaf, A. Hoser, T. Hofmann, and B. Keimer, Phys. Rev. B **85**, 184109 (2012).
[30] S. Ishiwata, M. Tokunaga, Y. Kaneko, D. Okuyama, Y. Tokunaga, S. Wakimoto, K. Kakurai, T. Arima, Y. Taguchi, and Y. Tokura, Phys. Rev. B **84**, 054427 (2011).
[31] F. J. Berry, R. Heap, O. Helgason, E. A. Moore, S. Shim, P. R. Slater, and M. F. Thomas, J. Phys.: Condens. Matter **20**, 215207 (2008).

[32] O. Clemens, F. J. Berry, A. J. Wright, K. S. Knight, J. M. Perez-Mato, J. M. Igartua, and P. R. Slater, J. Solid State Chem. **206**, 158 (2013).
[33] C. M. Thompson, C. K. Blakely, R. Flacau, J. E. Greedan, and V. V. Poltavets, J. Solid State Chem. **219**, 173 (2014).
[34] R. L. White, J. Appl. Phys. **40**, 1061 (1969).
[35] C. Greaves, A. J. Jacobson, B. C. Tofield, and B. E. F. Fender, Acta Crystallogr., Sect. B **31**, 641 (1975).
[36] E. J. Moon, Y. Xie, E. D. Laird, D. J. Keavney, C. Y. Li, and S. J. May, J. Am. Chem. Soc. **136**, 2224 (2014).
[37] T. Katayama, A. Chikamatsu, Y. Hirose, R. Takagi, H. Kamisaka, T. Fukumura, and T. Hasegawa, J. Mater. Chem. C **2**, 5350 (2014).
[38] P. R. Slater, J. Fluorine Chem. **117**, 43 (2002).
[39] Y. Kobayashi, M. Tian, M. Eguchi, and T. E. Mallouk, J. Am. Chem. Soc. **131**, 9849 (2009).
[40] S. Chakraverty, A. Ohtomo, M. Okude, K. Ueno, and M. Kawasaki, Cryst. Growth Des. **10**, 1725 (2010).
[41] See supplementary material at http://dx.doi.org/10.1063/1.4921579 for additional XPS data.
[42] M. D. Scafetta, Y. J. Xie, M. Torre, J. E. Spanier, and S. J. May, Appl. Phys. Lett. **102**, 081904 (2013).
[43] Y. Tsujimoto, K. Yamaura, N. Hayashi, K. Kodama, N. Igawa, Y. Matsushita, Y. Katsuya, Y. Shirako, M. Akaogi, and E. Takayama-Muromachi, Chem. Mater. **23**, 3652 (2011).
[44] M. V. Lovanov, A. M. Abakumov, A. V. Sidorova, M. G. Rozova, O. G. D'yachenko, E. V. Antipov, J. Hadermann, and G. Van Tendeloo, Solid State Sci. **4**, 19 (2002).
[45] O. Clemens, C. Rongeat, M. A. Reddy, A. Giehr, M. Fichtnerb, and H. Hahn, Dalton Trans. **43**, 15771 (2014).